2014 American Control Conference (ACC)
June 4-6, 2014. Portland, Oregon, USA

Stability Analysis of Connected Cruise Control with Stochastic Delays

Wubing B. Qin
Dept. of Mechanical Engineering
University of Michigan,
Ann Arbor, MI 48109, USA
Email: wubing@umich.edu

Marcella M. Gomez
Dept. of Mechanical Engineering
California Institute of Technology,
Pasadena, CA 91125, USA
Email: mgomez@caltech.edu

Gábor Orosz
Dept. of Mechanical Engineering
University of Michigan,
Ann Arbor, MI 48109, USA
Email: orosz@umich.edu

***Abstract*— In this paper we investigate the concept of connected cruise control (CCC) where vehicles rely on ad-hoc wireless vehicle-to-vehicle (V2V) communication to control their longitudinal motion. While V2V communication potentially allows vehicles to build detailed knowledge about the traffic environment, intermittencies and packet drops introduce stochastic delays into the communication channels that make control very challenging. Moreover, while communication and control occurs in discrete time, vehicle dynamics still takes place in continuous time. We convert the dynamics to discrete time and analyze the effects of stochastic delays on vehicular platoons. We derive plant and string stability conditions for the mean dynamics and show how the stable regimes shrink when the sampling time or the packet drop ratio increases. Our results have important implications regarding safety and efficiency of connected vehicle systems.**

I. INTRODUCTION

The last couple of decades have shown a huge improvement in driver assistance systems leading to vehicles that can control their lateral and longitudinal motion when driving in a structured environment (e.g., highway). The desired longitudinal motion is typically achieved by using adaptive cruise control (ACC) systems where the distance to the preceding vehicle is measured by a radar and the vehicle is actuated accordingly [1]. Apart from increasing driver comfort, such controllers were expected to have a positive impact on the overall traffic behavior [2]. However, mainly due to the cost of the radar, the penetration of ACC equipped vehicles is still very low.

Emerging technologies in wireless vehicle-to-vehicle (V2V) communication can lead to advanced driver assistance systems [3]. Such systems allow vehicles to obtain information about the motion of multiple vehicles ahead and may lead to more advanced longitudinal control, which can be implemented even when the vehicle is not equipped with a radar. We refer to this as connected cruise control (CCC) [4]. Apart from improving driver comfort and safety, the impact of CCC on traffic dynamics and mobility can be significant even for low penetration of CCC vehicles due to the long-range connections available [5, 6].

However, in CCC mode, packets are broadcasted every 100 ms using dedicated short range communication (DSRC) devices [3] and consequently digital effects and delays become significant [7]. Another difficulty arising in wireless communication is that packets may not be delivered successfully [8], resulting in stochastic delay variations. In this paper, we study the longitudinal dynamics of vehicles with stochastic delays in the communication channels and evaluate the stability of the uniform flow. In particular, we study plant stability, i.e., the ability of a CCC vehicle to follow a leader driving at a constant speed, and the string stability, that is, the ability of a CCC vehicle to attenuate velocity fluctuations imposed by the leader. String stability analysis allows one to extend stability results of a two-vehicle system to that of a platoon of vehicles. By analyzing the mean dynamics of the linearized system we derive necessary conditions for plant and string stability of vehicular platoons and evaluate the performance degradations when the packet delivery ratio decreases. We demonstrate by numerical simulations that the linear stability charts obtained for the mean dynamics provide information about the stability of the corresponding nonlinear stochastic system.

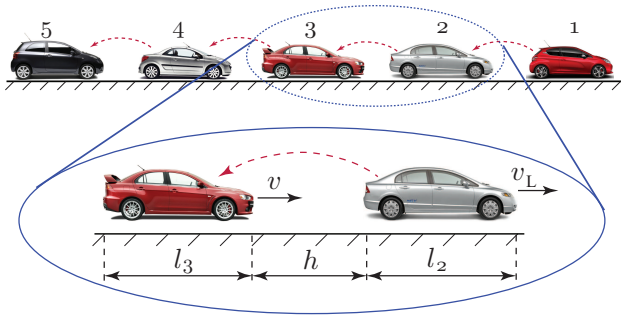

Fig. 1. The top row shows a platoon of cars equipped with wireless communication devices on a single lane, which is the concatenation of leader-follower configuration displayed at the bottom. Dashed arrows indicate wireless communication links between vehicles.

II. NONLINEAR MODEL WITH STOCHASTIC DELAY

In this section, a car-following model is extended in order to accommodate stochastic delay variations that occur in connected vehicle systems. Figure 1 shows a platoon where each vehicle is using the information sent by the car immediately ahead. This can be viewed as the concatenation of leader-follower pairs shown in Fig. 1. We consider a nonlinear controller that acts on the inter-vehicle distance (or headway) h, which can be calculated from GPS coordinates, the leader's velocity v_{L}, and the vehicle's own velocity v.

The leader broadcasts information intermittently with a

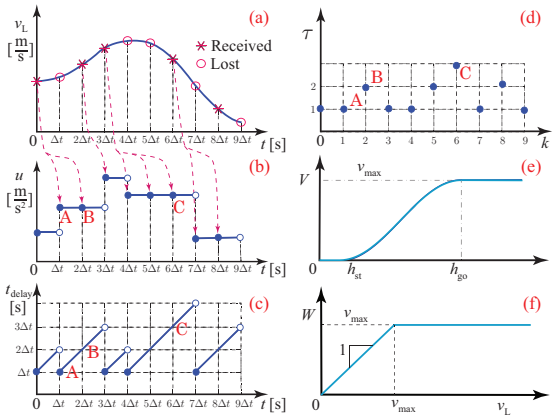

Fig. 2. (a) Leader's velocity is transmitted every Δt time, but packets may be dropped as indicated. (b) Controller output while using ZOH based on the newest received information. (c) Time delay variations arising in the controller. (d) Number of trials at different time instant $k\Delta t$. (e) Range policy function (7). (f) Saturation function (8).

sampling time of Δt, which yields the time mesh $t_k = k\Delta t$ for $k = 0, 1, 2, \ldots$; see Fig. 2(a). Let us denote the number of packets dropped at t_k as $\tau(k)-1$ where $\tau(k) \in \{1,\ 2,\ 3,\ \ldots\}$ represents the number of trials until a packet is delivered successfully. Suppose a packet is received successfully at $t = t_{k-\tau(k)}$, then the controller inputs a command at $t = t_{k-\tau(k)+1}$ based on this information. This input is kept constant until $t = t_{k+1}$ using a zero-order hold (ZOH) as the next successfully delivered packet will only be sent at $t = t_k$. Thus, the digitally controlled system is forced by piecewise constant inputs of stochastically varying length.

Fig. 2(d) shows the time evolution of $\tau(k)$, which can be formulated as

$$\tau(k+1) = \begin{cases} 1, & \text{if a packet is received} \\ & \text{during } [t_k,\, t_{k+1}); \\ \tau(k)+1, & \text{otherwise.} \end{cases} \tag{1}$$

Assuming that the packet delivery ratio is q, the corresponding probability density function of $\tau(k)$ is given by the geometric distribution

$$p_{\tau(k)}(\sigma) = \textstyle\sum_{r=1}^{\infty} w_r \delta(\sigma - r) \quad \text{with} \quad \sum_{r=1}^{\infty} w_r = 1\,, \tag{2}$$

where $\delta(*)$ denotes the Dirac delta function and

$$w_r = q(1-q)^{r-1}, \qquad r \in \{1\,,\, 2\,,\, 3\,,\, \ldots\}, \tag{3}$$

see [8, 9]. In order to avoid infinitely large delays, we truncate the distribution such that

$$w_r = \begin{cases} q(1-q)^{r-1} & \text{if} \quad r \in \{1\,,\, 2\,,\, \cdots\,,\, N-1\}\,, \\ 1 - \sum_{i=1}^{N-1} w_i = (1-q)^{N-1} & \text{if} \quad r = N\,, \\ 0 & \text{if} \quad r > N\,, \end{cases} \tag{4}$$

i.e., $\tau(k+1) = 1$ if $\tau(k) = N$, where N is the maximum number of trials. Also, $\sum_{r=1}^{N-1} w_r \geq p_{\rm cr}$ holds where $p_{\rm cr}$ is the critical cumulative delivery ratio. For example, based on the worst case scenario $q = 0.58$ presented in [8], using $p_{\rm cr} = 0.99$ the maximum value is $N = 6$.

For simplicity we consider zero inclination and omit rolling resistance and air drag effects, which leads to the simplified vehicle dynamics

$$\begin{aligned} \dot{h}(t) &= v_{\rm L}(t) - v(t)\,, \\ \dot{v}(t) &= u(t_{k-\tau(k)})\,, \end{aligned} \tag{5}$$

for $t_k \leq t < t_{k+1}$. We choose the nonlinear controller

$$u(t) = K_{\rm p}\Big(V\big(h(t)\big) - v(t)\Big) + K_{\rm v}\Big(W\big(v_{\rm L}(t)\big) - v(t)\Big)\,, \tag{6}$$

cf. [7].

Notice that since the dynamics of the vehicle still evolve in continuous time, the corresponding effective delay increases from $\tau(k)\Delta t$ to $\big(\tau(k)+1\big)\Delta t$ linearly during each sampling interval. Such stochastic delay variations are shown in Fig. 2(c). The points marked A, B and C in Fig. 2(b, c, d) illustrate the cases for $\tau(k) = 1$, 2 and 3, respectively.

The range policy $V(h)$ gives the desired velocity as a function of the headway h, and must be

- continuous and monotonously increasing (the more sparse traffic is, the faster the vehicles intend to run);
- zero for $h \leq h_{\rm st}$ (vehicles intend to stop within a safety distance);
- maximal for $h \geq h_{\rm go}$ (vehicles intend to run as fast as they can in sparse traffic – often referred to as free flow).

In this paper, we choose the continuously differentiable range policy

$$V(h) = \begin{cases} 0 & \text{if} \quad h < h_{\rm st}\,, \\ \dfrac{v_{\max}}{2}\Big(1 - \cos\big(\pi \frac{h-h_{\rm st}}{h_{\rm go}-h_{\rm st}}\big)\Big) & \text{if} \quad h_{\rm st} \leq h \leq h_{\rm go}\,, \\ v_{\max} & \text{if} \quad h > h_{\rm go}\,, \end{cases} \tag{7}$$

shown in Fig. 2(e). The saturation function $W(v_{\rm L})$ describes the switching between CCC mode ($v_{\rm L} \leq v_{\max}$) and normal cruise control mode ($v_{\rm L} > v_{\max}$) such that

$$W(v_{\rm L}) = \begin{cases} v_{\rm L} & \text{if} \quad v_{\rm L} \leq v_{\max}\,, \\ v_{\max} & \text{if} \quad v_{\rm L} > v_{\max}\,, \end{cases} \tag{8}$$

see Fig. 2(f).

For $v_{\rm L} \leq v_{\max}$ (CCC mode), system (5, 6) possesses the equilibrium

$$v_{\rm L}^* = v^* = V(h^*)\,. \tag{9}$$

Our goal is to design the control gains $K_{\rm p}\,,\, K_{\rm v}$ to ensure that the system can reach this equilibrium (i.e., plant stability is satisfied) and also attenuate perturbations introduced by the leader (i.e., string stability holds) in the presence of stochastic communication delays.

III. LINEARIZATION AND MEAN DYNAMICS

Solving the differential equation (5, 6) on the time interval $t \in [t_k,\ t_{k+1})$, one may create a discrete-time map, that is, fully discretize the dynamics. However, this is a difficult task due to the nonlinearities in the system. Therefore, we first linearize the system about the equilibrium (9) and discretize the obtained linear equations. Defining the perturbations

$\tilde{h}(t) = h(t) - h^*,\ \tilde{v}(t) = v(t) - v^*,\ \tilde{v}_{\rm L}(t) = v_{\rm L}(t) - v_{\rm L}^*$, we obtain

$$\begin{aligned}\begin{bmatrix}\dot{\tilde{h}}(t)\\ \dot{\tilde{v}}(t)\end{bmatrix} &= \begin{bmatrix}0 & -1\\ 0 & 0\end{bmatrix}\begin{bmatrix}\tilde{h}(t)\\ \tilde{v}(t)\end{bmatrix}\\ &+ \begin{bmatrix}0 & 0\\ K_{\rm p}N_* & -(K_{\rm p}+K_{\rm v})\end{bmatrix}\begin{bmatrix}\tilde{h}(t_{k-\tau(k)})\\ \tilde{v}(t_{k-\tau(k)})\end{bmatrix}\\ &+ \begin{bmatrix}1\\ 0\end{bmatrix}\tilde{v}_{\rm L}(t) + \begin{bmatrix}0\\ K_{\rm v}\end{bmatrix}\tilde{v}_{\rm L}(t_{k-\tau(k)})\,,\end{aligned} \tag{10}$$

for $t_k \le t < t_{k+1}$, where

$$\begin{aligned}N_* &= V'(h^*) = V'\big(V^{-1}(v^*)\big)\\ &= \begin{cases}\dfrac{\pi\sqrt{v^*(v_{\max}-v^*)}}{h_{\rm go}-h_{\rm st}} & \text{if} \quad h_{\rm st}\le h\le h_{\rm go}\,,\\ 0 & \text{elsewhere}\,,\end{cases}\end{aligned} \tag{11}$$

cf. (7).

Fourier's theory states that periodic signals can be represented as an infinite sum of sines and cosines, which can also be extended to quadratic integrable non-periodic signals. Henceforth, we will assume sinusoidal variations of the leader's velocity. Solving the linear equation (10) with input

$$\tilde{v}_{\rm L}(t) = \tilde{v}_{\rm L}^{\rm amp}\sin(\omega t) \tag{12}$$

along the time interval $[t_k,\, t_{k+1})$, one may derive the discrete-time map

$$\begin{aligned}X(k+1) &= \mathbf{A}\,X(k) + \mathbf{B}\,U(k)\\ &\quad + \mathbf{A}_\tau\,X\big(k-\tau(k)\big) + \mathbf{B}_\tau\,U\big(k-\tau(k)\big),\\ Y(k) &= \mathbf{C}\,X(k)\,,\end{aligned} \tag{13}$$

where the state, the output and the input are defined as

$$\begin{aligned}X(k) &= \begin{bmatrix}\tilde{h}(t_k)\\ \tilde{v}(t_k)\end{bmatrix}\,, \quad Y(k) = \tilde{v}(t_k)\,,\\ U(k) &= \begin{bmatrix}\tilde{v}_{\rm L1}(t_k)\\ \tilde{v}_{\rm L2}(t_k)\end{bmatrix} = \begin{bmatrix}\tilde{v}_{\rm L}^{\rm amp}\sin(k\omega\Delta t)\\ \tilde{v}_{\rm L}^{\rm amp}\cos(k\omega\Delta t)\end{bmatrix}\,,\end{aligned} \tag{14}$$

and the matrices are given by

$$\begin{aligned}\mathbf{A} &= \begin{bmatrix}1 & -\Delta t\\ 0 & 1\end{bmatrix}, \quad \mathbf{B} = \begin{bmatrix}\alpha_1 & \alpha_2\\ 0 & 0\end{bmatrix},\\ \mathbf{A}_\tau &= \begin{bmatrix}-\frac{1}{2}\Delta t^2 K_{\rm p}N_* & \frac{1}{2}\Delta t^2(K_{\rm p}+K_{\rm v})\\ \Delta t K_{\rm p}N_* & -\Delta t(K_{\rm p}+K_{\rm v})\end{bmatrix},\\ \mathbf{B}_\tau &= \begin{bmatrix}-\frac{1}{2}\Delta t^2 K_{\rm v} & 0\\ \Delta t K_{\rm v} & 0\end{bmatrix}, \quad \mathbf{C} = \begin{bmatrix}0 & 1\end{bmatrix},\end{aligned} \tag{15}$$

where

$$\alpha_1 = \frac{\sin(\omega\Delta t)}{\omega}\,, \quad \alpha_2 = \frac{1-\cos(\omega\Delta t)}{\omega}. \tag{16}$$

That is, in the discrete-time system (13), $\tau(k)$ plays the role of a discrete stochastic delay, see Fig. 2(d). Notice that the scalar sinusoidal input (12) that drives the continuous-time system (10) results in the vector-valued input in (14) for the discrete-time system (13). Also notice that

$$U(k-r) = \mathbf{R}^r\,U(k), \tag{17}$$

where

$$\mathbf{R} = \begin{bmatrix}\cos(\omega\Delta t) & -\sin(\omega\Delta t)\\ \sin(\omega\Delta t) & \cos(\omega\Delta t)\end{bmatrix}. \tag{18}$$

Defining the $2(N+1)$-dimensional augmented state

$$\hat{X}(k) = \begin{bmatrix}X(k)\\ X(k-1)\\ \vdots\\ X(k-N)\end{bmatrix}, \tag{19}$$

(13) can be written as

$$\begin{aligned}\hat{X}(k+1) &= \hat{\mathbf{A}}_{\tau(k)}\,\hat{X}(k) + \hat{\mathbf{B}}_{\tau(k)}\,U(k),\\ Y(k) &= \hat{\mathbf{C}}\,\hat{X}(k)\,,\end{aligned} \tag{20}$$

where $\hat{\mathbf{A}}_{\tau(k)} \in \mathbb{R}^{2(N+1)\times 2(N+1)}$ and $\hat{\mathbf{B}}_{\tau(k)} \in \mathbb{R}^{2(N+1)\times 2}$ can take the values

$$\begin{aligned}\hat{\mathbf{A}}_r &= \begin{bmatrix}\mathbf{A} & \lambda_1(r)\,\mathbf{A}_\tau & \lambda_2(r)\,\mathbf{A}_\tau & \cdots & \lambda_N(r)\,\mathbf{A}_\tau\\ \mathbf{I} & \mathbf{0} & \mathbf{0} & \cdots & \mathbf{0}\\ \mathbf{0} & \mathbf{I} & \mathbf{0} & \cdots & \mathbf{0}\\ \vdots & & \ddots & \ddots & \vdots\\ \mathbf{0} & \cdots & \mathbf{0} & \mathbf{I} & \mathbf{0}\end{bmatrix},\\ \hat{\mathbf{B}}_r &= \begin{bmatrix}\mathbf{B}+\mathbf{B}_\tau\,\mathbf{R}^r\\ \mathbf{0}\\ \vdots\\ \mathbf{0}\end{bmatrix},\end{aligned} \tag{21}$$

for $r = 1, 2, \cdots, N$, cf. (15). Here, $\lambda_i(r)$ denotes the indicator function such that

$$\lambda_i(r) = \begin{cases}0\,, & r\ne i,\\ 1\,, & r = i,\end{cases} \qquad i\in\{1,\,2,\,\ldots,\,N\}, \tag{22}$$

while $\mathbf{I} \in \mathbb{R}^{2\times 2}, \mathbf{0} \in \mathbb{R}^{2\times 2}$ denote identity and zero matrices, respectively. Also we have

$$\hat{\mathbf{C}} = \begin{bmatrix}\mathbf{C} & \mathbf{0}' & \cdots & \mathbf{0}'\end{bmatrix}, \tag{23}$$

where $\hat{\mathbf{C}} \in \mathbb{R}^{1\times 2(N+1)}$, and $\mathbf{0}' = \begin{bmatrix}0 & 0\end{bmatrix}$. In (20), $\hat{\mathbf{A}}_{\tau(k)}$ depends on $\hat{\mathbf{A}}_{\tau(k-1)}$ according to (1, 2, 4), which also holds for $\hat{\mathbf{B}}_{\tau(k)}$ and $\hat{\mathbf{B}}_{\tau(k-1)}$, implying that (20) is a non-Markovian stochastic process.

Let us consider the states at time instants that correspond to k-s where $\tau(k) = 1$, cf. Fig 2(d), that is, where a packet is delivered, and define a new couter l for these points. Using (20) recursively between such points, we can obtain

$$\begin{aligned}\hat{X}(l+1) &= \hat{\mathbf{G}}(l)\,\hat{X}(l) + \hat{\mathbf{H}}(l)\,U(l),\\ Y(l) &= \hat{\mathbf{C}}\,\hat{X}(l)\,,\end{aligned} \tag{24}$$

where $\hat{\mathbf{G}}(l) \in \mathbb{R}^{2(N+1)\times 2(N+1)}$ and $\hat{\mathbf{H}}(l) \in \mathbb{R}^{2(N+1)\times 2}$ can take values given by

$$\begin{aligned}\hat{\mathbf{G}}_r &= \prod_{i=1}^{r}\hat{\mathbf{A}}_i\,, \qquad r = 1,\,2,\,\ldots,\,N\,,\\ \hat{\mathbf{H}}_r &= \begin{cases}\hat{\mathbf{B}}_1, & r = 1,\\ \hat{\mathbf{A}}_r\hat{\mathbf{H}}_{r-1} + \hat{\mathbf{B}}_r\big(\mathbf{R}^{-1}\big)^{r-1}, & r\in\{2,\,3\,\ldots,N\}.\end{cases}\end{aligned} \tag{25}$$

In (24), $\hat{\mathbf{G}}(l)$ at each time instant l is independently, identically distributed (i.i.d.), which also holds for $\hat{\mathbf{H}}(l)$, meaning that (24) is indeed a discrete-time stochastic Markov process. Also, $\hat{\mathbf{G}}(l)$ and $\hat{\mathbf{H}}(l)$ satisfy

$$\begin{aligned} p_{\hat{\mathbf{G}}(l)}(\hat{\mathbf{G}}) &= \textstyle\sum_{r=1}^{\infty} w_r \delta(\hat{\mathbf{G}} - \hat{\mathbf{G}}_r)\,, \\ p_{\hat{\mathbf{H}}(l)}(\hat{\mathbf{H}}) &= \textstyle\sum_{r=1}^{\infty} w_r \delta(\hat{\mathbf{H}} - \hat{\mathbf{H}}_r)\,, \end{aligned} \tag{26}$$

where w_r is given by (4) and $\delta(*)$ denotes the Dirac delta function. It can also be proven that the stochastic system (20) subject to (1, 2, 4) is stable if and only if the system (24) subject to (26) is stable.

It is known that a linear stochastic discrete-time system is pointwise asymptotically stable if and only if its second moment dynamics are stable [10]. Moreover, the stability of the second moment implies stability of the mean. In the following analysis, the stability conditions for the mean dynamics will be derived. This provides us with a necessary condition for stability that is often close to the necessary and sufficient condition given by the second moment [11]. Results will also be presented in the case when the system is forced periodically and string stability conditions for the mean dynamics will be derived.

Let us define the deterministic variables

$$\bar{X}(l) = E[\hat{X}(l)]\,,\;\; \bar{Y}(l) = E[Y(l)]\,. \tag{27}$$

By taking expectations of both sides in (24), one can derive the equation describing the mean dynamics

$$\begin{aligned} \bar{X}(l+1) &= \bar{\mathbf{G}}\,\bar{X}(l) + \bar{\mathbf{H}}\,U(l)\,, \\ \bar{Y}(l) &= \bar{\mathbf{C}}\,\bar{X}(l)\,, \end{aligned} \tag{28}$$

where

$$\bar{\mathbf{G}} = \sum_{r=1}^{N} w_r \hat{\mathbf{G}}_r\,,\quad \bar{\mathbf{H}} = \sum_{r=1}^{N} w_r \hat{\mathbf{H}}_r\,,\quad \bar{\mathbf{C}} = \hat{\mathbf{C}}, \tag{29}$$

cf. [9, 11].

IV. Stability Analysis

In this section, plant stability and string stability conditions for the mean dynamics (28) are provided as an approximation to the corresponding exact plant and string stability domains of the stochastic system (24). Plant stability means that the follower is capable of approaching the leader's velocity when the leader is driving at a constant velocity. String stability means that the follower is capable of attenuating perturbations in the leader's velocity. Since superposition holds for linear systems, string stability is equivalent to the attenuation of sinusoidal signals at all frequencies [12].

A. Necessary Condition for Plant Stability

For plant stability of the mean dynamics, all the eigenvalues of the corresponding system matrix $\bar{\mathbf{G}}$ in (29) must lie within the unit circle in the complex plane. The characteristic equation is

$$f(z) = \det(z\,\bar{\mathbf{I}} - \bar{\mathbf{G}}) = 0\,, \tag{30}$$

where $z \in \mathbb{C}$, and $\bar{\mathbf{I}} \in \mathbb{R}^{2(N+1)\times 2(N+1)}$ is the identity matrix.

It is known that a discrete-time system can lose its stability in three qualitatively different ways [13]: a real eigenvalue crosses the unit circle at 1, a real eigenvalue crosses the unit circle at -1, or a pair of complex conjugate eigenvalues crosses the unit circle. Thus, by substituting these critical eigenvalues into (30), the linear plant stability boundaries can be obtained in parameter space as

$$z = 1 \qquad \Longleftrightarrow f_1(K_\mathrm{p}, K_\mathrm{v}, v^*, w, \Delta t) = 0\,, \tag{31}$$

$$z = -1 \qquad \Longleftrightarrow f_2(K_\mathrm{p}, K_\mathrm{v}, v^*, w, \Delta t) = 0\,, \tag{32}$$

$$z = \mathrm{e}^{j\Omega_\mathrm{cr}\Delta t} \quad \Longleftrightarrow \begin{cases} f_3(K_\mathrm{p}, K_\mathrm{v}, v^*, w, \Delta t, \Omega_\mathrm{cr}) = 0\,, \\ f_4(K_\mathrm{p}, K_\mathrm{v}, v^*, w, \Delta t, \Omega_\mathrm{cr}) = 0\,, \end{cases} \tag{33}$$

where w denotes the set of all the w_r-s for $r \in \{1, 2, \cdots, N\}$, and Ω_cr denotes the critical angular frequencies at which plant stability changes. Solving these for K_p and K_v, one may obtain the stability boundaries. In case of (33), these are parameterized by Ω_cr.

Fig. 3 shows the stability charts in the $(K_\mathrm{v},\, K_\mathrm{p})$-plane for different values of the packet delivery ratio q and sampling time Δt. The inlets show the probability distribution of discrete stochastic delay given by (2). Solid red curves represent plant stability boundaries, and the lobe-shaped shaded domains (both light gray and dark gray) are plant stable. (The solid blue curves and the lobe-shaped dark gray regions will be explained in section IV-B.) The plant stable domain shrinks as the packet delivery ratio q decreases and as sampling ratio Δt increases. The oscillation frequency is zero along the horizontal red line given by (31) while the frequency Ω_cr increases monotonously along the other stability curve given by (33), that is, the further we are from the origin (along the curve), the higher the frequency of the arising oscillation is.

B. Necessary Condition for String Stability

For string stability, we consider $\tilde{v}(t)$ as output corresponding to periodic input (12). After discretizing time (cf. (13), (14)), we obtain two discrete inputs $\tilde{v}_{\mathrm{L}1}(t_k) = \tilde{v}_{\mathrm{L}1}(k)$ and $\tilde{v}_{\mathrm{L}2}(t_k) = \tilde{v}_{\mathrm{L}2}(k)$, and one discrete output $\tilde{v}(t_k) = \tilde{v}(k)$. Then we apply Z transform and use (28) and (29) to obtain the corresponding transfer function

$$\Gamma(z) = [\gamma_1(z) \quad \gamma_2(z)] = \bar{\mathbf{C}}\big(z\,\bar{\mathbf{I}} - \bar{\mathbf{G}}\big)^{-1}\bar{\mathbf{H}}. \tag{34}$$

To simplify the notations, γ_1 and γ_2 will be used in lieu of $\gamma_1(e^{j\omega\Delta t})$ and $\gamma_2(e^{j\omega\Delta t})$, respectively. In discrete linear time invariant systems, the steady state output of $\tilde{v}(k)$ can be expressed as the summation of the contribution of each individual input given by (34). By applying trigonometric identities and Euler's formula, the steady state output can be

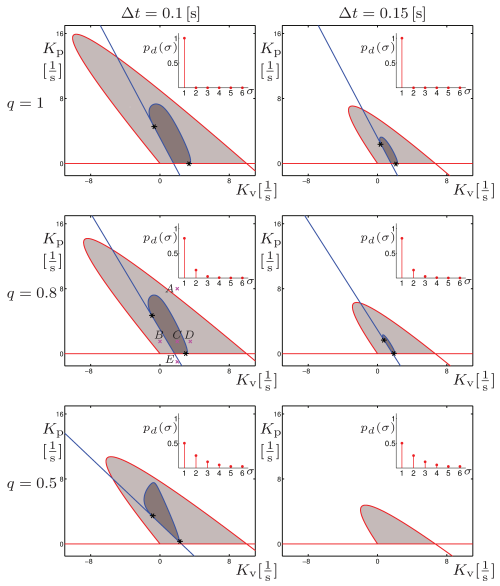

Fig. 3. Stability diagrams in the (K_v, K_p)-plane for $v_{max} = 30$ m/s, $h_{st} = 5$ m, $h_{go} = 35$ m, $v^* = 15$ m/s (cf. (7), (9)) and different values of packet delivery ratio q and sampling time Δt as indicated. The corresponding delay distributions (2) are plotted on each panel as inlets. Red and blue curves correspond to changes in plant and string stability, respectively. Dark gray regions represent parameters where the system is plant and string stable, while in the light gray regions only plant stability is achieved.

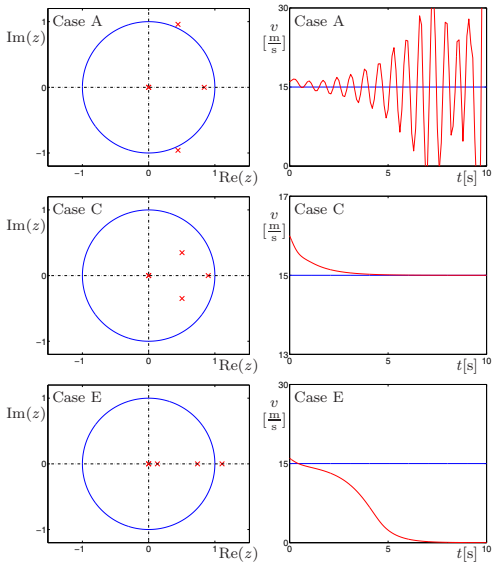

Fig. 4. Left column: Root loci on the z-domain corresponding to the points A, C and E in Fig. 3. Right column: Mean of 1000 simulations for the nonlinear system (5) subject to constant input $v_L(t) \equiv v_L^*$. The initial perturbations are $\tilde{h}(t) = 1$ m, $\tilde{v}(t) = 1$ m/s, for $t \in [-\Delta t\,, 0]$. Blue and red curves represent the leader's and the follower's velocities, respectively.

written as

$$\begin{aligned}\tilde{v}_{ss}(k) &= |\gamma_1|\tilde{v}_L^{amp}\sin(k\omega\Delta t + \angle\gamma_1)\\ &\quad + |\gamma_2|\tilde{v}_L^{amp}\cos(k\omega\Delta t + \angle\gamma_2)\\ &= \Big(\mathrm{Re}(\gamma_1) - \mathrm{Im}(\gamma_2)\Big)\tilde{v}_L^{amp}\sin(k\omega\Delta t)\\ &\quad + \Big(\mathrm{Im}(\gamma_1) + \mathrm{Re}(\gamma_2)\Big)\tilde{v}_L^{amp}\cos(k\omega\Delta t)\\ &= |\Gamma_{cmp}|\tilde{v}_L^{amp}\sin(k\omega\Delta t + \psi),\end{aligned} \tag{35}$$

where

$$|\Gamma_{cmp}| = \sqrt{|\gamma_1|^2 + |\gamma_2|^2 + 2\mathrm{Im}(\gamma_1\overline{\gamma}_2)}\,, \tag{36}$$

is the magnitude and ψ is the phase lag at frequency ω.

In order to be string stable, the maximum of $|\Gamma_{cmp}|^2$ must be less than 1. Thus, the string stability boundaries in the parameter space are given by

$$\begin{cases} |\Gamma_{cmp}(\omega_{cr})| = 1, \\ \dfrac{\mathrm{d}|\Gamma_{cmp}|}{\mathrm{d}\omega}\Big|_{\omega_{cr}} = 0, \end{cases} \tag{37}$$

for $\omega_{cr} > 0$ where $|\Gamma_{cmp}|$ also depends on other parameters, i.e., $|\Gamma_{cmp}| = |\Gamma_{cmp}(K_p, K_v, w, v^*, \Delta t, \omega)|$. For $\omega_{cr} = 0$, we obtain the other boundaries (see [7])

$$K_p = 0, \tag{38}$$

$$K_p = g(K_v,\, w\,,\, v^*,\, \Delta t), \tag{39}$$

while for $\omega_{cr} > 0$, the stability curves are parameterized by ω_{cr}.

In Fig. 3, the string stability boundaries are plotted in the (K_v, K_p)-plane as solid blue curves for different values of the packet delivery ratio q and sampling time Δt. Dark gray islands correspond to string stable regions and these are embedded in the light gray plant stable domains. We remark that there are some other string stability boundaries outside the plant stable domain which are not shown here. The string stable domains also shrink when packet delivery ratio q decreases or the sampling time Δt increases. When exceeding critical values, the domains disappear, in which case there exist no gain combinations that can maintain string stability. The frequency is zero along the straight lines given by (38) and (39) and ω_{cr} increases as we move away from the black stars along the curve given by (37) (i.e., string stability is lost at higher frequencies).

V. Simulation Results

In this section, we use numerical simulations to demonstrate the stability results generated above. We show that the necessary conditions of linear stability obtained above can give a guidance when selecting control gains to achieve the desired behavior.

A. Plant Stability Simulations

The root loci given by (30) and the mean of 1000 numerical simulations of the stochastic system (5, 6) without periodic forcing (i.e., $\tilde{v}_L^{amp} = 0$), are plotted in Fig. 4. Note that the integration time step is chosen to be $\Delta t/10$. Cases A, C and E correspond to the points marked in the panel corresponding to $q = 0.8\,, \Delta t = 0.1\,\mathrm{s}$ in Fig. 3 at $K_v = 2\,\mathrm{s}^{-1}$.

In case A (top panels), a pair of complex conjugate eigenvalues is located outside the unit circle, and simulation results show that oscillations arise with frequency corresponding to those complex conjugate eigenvalues. As K_p

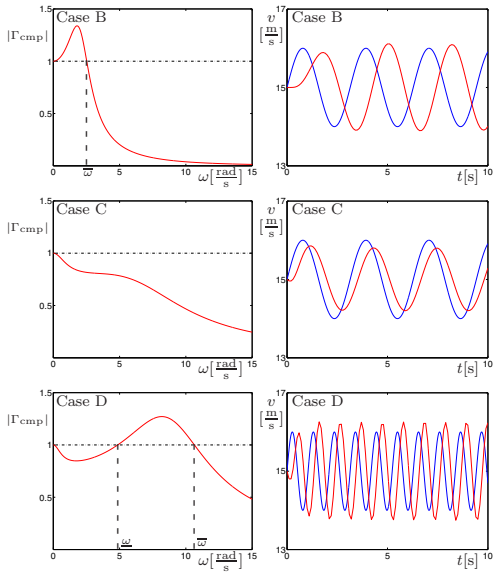

Fig. 5. Left column: output-input amplitude ratios as a function of the excitation frequency ω corresponding to the points B, C and D in Fig. 3. Right column: mean of 1000 simulations of the nonlinear system (5) subject to sinusoidal input (12) with $v_{\rm L}^* = 15\,{\rm m/s}$, $\tilde{v}_{\rm L}^{\rm amp} = 1\,{\rm m/s}$. Here, $\omega = 2\,{\rm rad/s}$ for the first two rows, $\omega = 6\,{\rm rad/s}$ for the third row. Blue and red curves represent the leader's and follower's velocities, respectively. The initial conditions are chosen as $\tilde{h}(t) = 0$ m, $\tilde{v}(t) = 0$ m/s, for $t \in [-\Delta t\,,\,0]$.

decreases, the eigenvalues move inside the unit circle as shown by case C (middle row). In this case, the system approaches the equilibrium as demonstrated by numerical simulations. Decreasing $K_{\rm p}$ further, the pair of complex conjugate eigenvalues "meet" at the real axis and then they split into two real eigenvalues. One of them crosses the unit circle at 1 and moves outside as shown in Case E (bottom panels). The corresponding simulations show loss of mean plant stability without oscillations.

B. String Stability Simulations

The magnitude of transfer function (36) and the mean of 1000 numerical simulations of the stochastic system (5, 6) with periodic forcing (12) (i.e., $\tilde{v}_{\rm L}^{\rm amp} \neq 0$), are plotted in Fig. 5. Cases B, C and D correspond to the points marked in the panel corresponding to $q = 0.8\,,\ \Delta t = 0.1\,{\rm s}$ in Fig. 3 at $K_{\rm p} = 1.5\,{\rm s}^{-1}$.

In case B (top panels) the system is mean string unstable for $0 < \omega < \overline{\omega}$, but string stable elsewhere. The corresponding simulations show that amplification happens for excitation frequency $\omega = 2\,{\rm rad/s}$. As $K_{\rm v}$ increases, the magnitude of the transfer function goes below 1 for all frequencies. In case C (middle row) the system is mean string stable, and the corresponding simulation shows that the amplitude of the sinusoidal input with excitation frequency $\omega = 2\,{\rm rad/s}$ is attenuated. However, as $K_{\rm v}$ increases further and we move outside the string stability domain, another peak of the transfer function arises. The bottom left panel shows that the system is mean string unstable for $\underline{\omega} < \omega < \overline{\omega}$, but string stable elsewhere. The corresponding simulations show that the amplitude of sinusoidal input with excitation frequency $\omega = 6\,{\rm rad/s} \in (\underline{\omega}, \overline{\omega})$ is amplified. Corresponding to the stochastic nature of packet drops, simulations show amplitude variations which are "not uniformly" string unstable. We remark that in some cases simulations show string stable behavior where analytical results predict high frequency ($\omega \geq 6\,{\rm rad/s}$) string instability. This is because high frequency signals are filtered by the low sampling rates ($\Delta t \geq 0.1\,{\rm s}$). Investigating such effects is left for future research.

VI. CONCLUSIONS

In this paper, the effects of stochastic delays on the dynamics of connected vehicles were studied by analyzing the mean dynamics. Both plant and string stability conditions were derived and it was shown that the stability domains shrink when the packet drop ratio or the sampling time increases. Furthermore, above a critical limit string stability cannot be achieved by any gain combinations. Our future research will include derivation of string stability conditions using the second moment and shaping the delay distributions in order to improve stability.

ACKNOWLEDGMENT

This work was supported in part by NSF grant 1300319 and the TerraSwarm Research Center, one of six centers supported by the STARnet phase of the Focus Center Research Program (FCRP) a Semiconductor Research Corporation program sponsored by MARCO and DARPA.

REFERENCES

[1] S. E. Shladover, "Longitudinal control of automotive vehicles in close-formation platoons," *Journal of Dynamic Systems, Measurement, and Control*, vol. 113, no. 2, 1991.
[2] L. C. Davis, "Effect of adaptive cruise control systems on traffic flow," *Physical Review E*, vol. 69, no. 6, p. 066110, 2004.
[3] D. Caveney, "Cooperative vehicular safety applications," *IEEE Control Systems Magazine*, vol. 30, no. 4, pp. 38–53, 2010.
[4] G. Orosz, "Connected cruise control: modeling, delay effects, and nonlinear behavior," *Vehicle System Dynamics*, p. submitted, 2014.
[5] J. I. Ge, S. S. Avedisov, and G. Orosz, "Stability of connected vehicle platoons with delayed acceleration feedback," in *Proceedings of the ASME Dynamical Systems and Control Conference*. ASME, 2013.
[6] L. Zhang and G. Orosz, "Designing network motifs in connected vehicle systems: delay effects and stability," in *Proceedings of the ASME Dynamical Systems and Control Conference*. ASME, 2013.
[7] W. B. Qin and G. Orosz, "Digital effects and delays in connected vehicles: Linear stability and simulations," in *Proceedings of the ASME Dynamical Systems and Control Conference*. ASME, 2013.
[8] F. Bai and H. Krishnan, "Reliability analysis of dsrc wireless communication for vehicle safety applications," in *Proceedings of the IEEE Intelligent Transportation Systems Conference*. IEEE, 2006.
[9] M. M. Gomez, G. Orosz, and R. M. Murray, "Stability of discrete-time systems with stochastically delayed feedback," in *European Control Conference*, pp. 2609 – 2614.
[10] H. Kushner, *Introduction to Stochastic Control*. Holt, Rinehart and Winston, Inc., 1971.
[11] M. M. Gomez, W. B. Qin, G. Orosz, and R. M. Murray, "Exact stability analysis of discrete-time linear systems with stochastic delays," in *Proceedings of American Control Conference*, 2014.
[12] D. Swaroop and J. K. Hedrick, "String stability of interconnected systems," *IEEE Transactions on Automatic Control*, vol. 41, no. 3, pp. 349–357, 1996.
[13] J. Guckenheimer and P. Holmes, *Nonlinear Oscillations, Dynamical Systems, and Bifurcations of Vector Fields*. Springer-Verlag, 1983, no. 42.